# Dura-mater Under Repetitive Analysis for Formulation of a Rheological Model - DURA-FORM

## 1 Research project objectives

The primary objective of the **DURA-FORM** project will be to develop strain-rate dependent constitutive law for the human spinal dura mater, reflecting its complex, anisotropic mechanical behavior under loading and the rheological effects. By combining systematic experimental measurements, such as uniaxial tensile tests, cyclic loading (to capture the Mullins effect and hysteresis), and high-rate dynamic evaluations, with advanced finite element (FE) modeling, the project will aim to elucidate how the cyclic, anisotropic, and viscoelastic properties of the dura mater influence injury mechanisms during high-impact events (e.g., road collisions). A comprehensive understanding of these processes will enable the refinement of existing Human Body Models (HBMs) and will guide clinical and engineering strategies to mitigate spinal cord injuries. Particular Goals (PGs):

**PG1:** Quantify the anisotropic material behavior of the spinal dura mater under varying strain rates, encompassing static and dynamic uniaxial and cycling testing protocols. Assess phenomena such as the Mullins effect and hysteresis arising from repetitive loading. This particular goal will be achieved in cooperation with Medical University of Gdańsk (GUMed).

**PG2:** Formulate advanced material models that capture the dura mater's fiber-reinforced structure and time-dependent (viscous) properties for both small and large deformations. Validate these models using full-field deformation data obtained via digital image correlation (DIC).

**PG3:** Integrate the new anisotropic, rate-dependent models into commercial FE software (e.g., LS-DYNA). Evaluate their predictive capabilities across a spectrum of loading conditions, from low-rate quasi-static tests to high-impact crash simulations.

**PG4:** Combine simulation data with experimental results to determine critical thresholds and injury risk metrics for dural failure, focusing on parameters such as failure stress and failure strain. Investigate the specific conditions under which these endurance limits may be exceeded. This particular goal will be achieved in cooperation with GUMed.

Through this integrated experimental–computational approach, the DURA-FORM project will significantly advance understanding of spinal dura mater mechanics, laying the groundwork for innovative engineering solutions and evidence-based clinical interventions to protect the spinal cord during high-impact scenarios.

## 2 Significance of the project

The **DURA-FORM** project will address gaps in understanding the mechanical behavior of the human spinal dura mater under daily activities and high-impact events. By developing and refining FE methods, the project will seek to advance both clinical and engineering strategies for protecting the spinal cord and reducing injury risks.

### 2.1 State of the art

Encircled by three protective meningeal layers, the spinal cord transmits nerve impulses between the brain and the body [1,2]. Among these layers, the dura mater, rich in collagen, forms a protective barrier that helps maintain cerebrospinal fluid (CSF) pressure and shields neural elements from mechanical loads [3,4]. Although thinner than its cranial counterpart, the spinal dura is firmly anchored to the surrounding vertebrae via fibrous extensions, limiting excessive cord motion and contributing to spinal stability [5,6]. Disruptions of this membrane, whether due to trauma, invasive procedures, or degenerative changes, may lead to severe neurological deficits or persistent CSF leakage [7,8]. These clinical concerns have spurred extensive biomechanical investigations into dural responses under different loading conditions [9].

A wide range of experiments has been conducted to assess the mechanical properties of the spinal dura mater, with uniaxial tension tests being prominent [10–14]. In these studies, a rectangular or dog-bone-shaped sample is stretched at a prescribed rate until failure, yielding data on stiffness, ultimate tensile strength, and strain at rupture [15]. However, the tissue's thin profile, pronounced anisotropy, and variable collagen fiber orientation complicate uniaxial testing [16]. Moreover, donor-specific factors, including age, sex, and pathological history, often influence mechanical outcomes [13,14]. Such variability emphasizes the need for standardized protocols covering tissue harvesting, preservation, and testing [17,18].

Beyond monotonic loading, cyclic loading protocols have gained attention for revealing viscoelastic tissue characteristics [19,20]. Two key phenomena often observed under cyclic loading are the Mullins effect and hysteresis [21–23]. The Mullins effect is an irreversible stress-softening that appears whenever a rubber-like material is loaded beyond its previous maximum strain; after each new peak load, subsequent loading-unloading cycles follow a reduced-stiffness stress–strain path [24]. Hysteresis represents energy loss between loading and unloading curves, forming a loop on stress–strain diagrams. Both phenomena hold practical

importance for scenarios involving repeated or sub-failure loading, such as moderate impacts, vibrations, or certain neurosurgical manipulations [6]. However, research specifically focused on cyclic testing of human spinal dura is limited, leaving open questions about preconditioning protocols and the potential for damage under repeated loading [16,25].

Strain-rate sensitivity further complicates dural behavior. While most early investigations were performed at slow or quasi-static rates [11,12,14], real-life circumstances such as automobile collisions or sports impacts impose higher strain rates [26]. Recent findings suggest that biological tissues, including dura mater, can exhibit markedly increased stiffness and strength at elevated loading rates [27,28]. Yet comprehensive data for spinal dura in the range of 0.1 $s^{-1}$ to 100 $s^{-1}$ remain sparse [29]. This gap has notable implications for injury biomechanics, if the dura stiffens under rapid deformation, it may convey larger loads to the spinal cord, potentially exacerbating neural trauma [4].

In addition to ultimate strength and strain-rate dependence, the apparent Poisson's ratio offers further insights into dural deformation mechanics [30,31]. Although many soft tissues are often treated as nearly incompressible, the spine's dura mater may deviate from this assumption due to its dense collagen fibers and anisotropy [32]. Reliable estimates of transverse-to-axial strain ratios are thus integral to more realistic numerical simulations. Traditional uniaxial tests relying solely on crosshead displacement might misrepresent Poisson's ratio by overlooking local strain variations [33]. In contrast, optical techniques like DIC can accurately map strain fields across the tissue surface, distinguishing between machine-based and tissue-based deformations [34,35]. Despite practical hurdles, such as speckle application and camera synchronization, DIC is particularly valuable for thin, anisotropic tissues where clamping-based measurements often prove less reliable [36,37].

Constitutive modeling connects these experimental insights to large-scale FE simulations. HBMs, such as VIVA [38] and THUMS [39], include increasingly detailed musculoskeletal and soft tissue structures [40,41]. However, the dura is typically represented as a simplified linear-elastic material, omitting viscoelastic or fiber-reinforced traits [26]. This omission may yield inaccuracies in high-speed crash simulations, where strain-rate dependencies and nonlinear stress–strain relationships strongly influence injury outcomes [42]. By integrating visco-hyperelastic or transversely isotropic formulations that capture the Mullins effect, hysteresis, and strain-rate effects, researchers can more accurately represent the mechanical environment surrounding the spinal cord [43,44]. Validated material models can then be incorporated into HBMs to predict dural tears or spinal cord compromise in high-impact events [45,46].

Summarizing, the present project aims to improve the understanding of uniaxial, cyclic, and rate-dependent properties of the human spinal dura mater. By combining experiments, including low and high strain loading, sub-failure cyclic tension, and DIC-based strain measurements, with advanced numerical modeling, this work seeks to:

- **(i)** characterize mechanical responses over a broad range of strain rates,
- **(ii)** quantify the Mullins effect and hysteresis under cyclic loading,
- **(iii)** refine estimates of the apparent Poisson's ratio, and
- **(iv)** develop constitutive models that capture these behaviors.

### 2.2 Justification for tackling specific scientific problems by the proposed project

Developing a comprehensive mathematical model supported by experimental studies and statistical analysis, this project will address a gap in understanding the biomechanical mechanisms. The proposed research on the rate-dependent, cyclic, and nonlinear mechanical properties of the human spinal dura mater stems from insufficient knowledge about spinal biomechanics, particularly in high-impact or repetitive loading contexts. While many studies focus on vertebral bodies, intervertebral discs, and ligaments, the dura mater, a vital membrane protecting the spinal cord, remains underexplored regarding its detailed mechanical response. Past investigations often limit testing to low strain rates or single loading–unloading cycles, overlooking viscoelastic phenomena such as the Mullins effect and hysteresis that become especially relevant under repeated loading.

The first scientific challenge addressed by this project is the comprehensive characterization of the dura mater under strain rates that approximate traumatic or high-speed scenarios, such as vehicular crashes, sports activities or bungee jumping. Rapid deformations at these higher rates can significantly alter tensile properties, potentially increasing stiffness and ultimate strength. In the absence of robust, high-rate mechanical data, FE models and HBMs may misrepresent spinal cord injury risk, resulting in inaccurate predictions of neuromechanical compromise under dynamic loading conditions.

A second challenge concerns the effects of repeated sub-failure loading. Clinically, the spinal dura can experience repetitive tensile or vibrational loads, for example, in certain surgical procedures or in situations involving multiple minor collisions. These circumstances raise questions about stress-softening, hysteresis, and other viscoelastic responses that standard static tests do not capture. Quantifying the Mullins effect is vital

to determine whether and how the dura exhibits decreasing stiffness after initial stretches, which may have implications for understanding progressive weakening of meningeal tissues and the increased susceptibility to rupture or tearing over time.

A third, closely related scientific need is to clarify the dura's apparent Poisson's ratio under realistic loading conditions. Traditional mechanical tests often rely exclusively on crosshead displacement data, potentially obscuring local deformation patterns. By integrating DIC, this project will resolve strain distributions with high spatial resolution, enabling more accurate modeling of the transverse–axial strain relationship and improving the constitutive models that govern predictive simulations.

Finally, the project's emphasis on integrating experimental data with advanced constitutive modeling directly targets the gap between bench-top research and real-world applications. Existing HBMs typically treat the spinal dura as a simplified linear-elastic material, neglecting important rate- and cycle-dependent characteristics. By generating validated visco-hyperelastic formulations, this research will advance these models for greater fidelity.

Overall, the project is scientifically justified in addressing these problems because it offers a comprehensive strategy: precise mechanical testing across multiple loading scenarios, development of refined constitutive laws, and validation within FE environments. This holistic approach will provide the mechanical behavior of the spinal dura mater, facilitating more accurate injury predictions and improved therapeutic or preventive measures.

### 2.3 Novelty of the project

The research will integrates multiple innovative approaches and will address gaps in the current understanding of spinal dura mater biomechanics:

- **Multi-Rate Experimental Framework:** While previous investigations have primarily focused on quasi-static or low-strain-rate conditions, the present study will systematically examine higher strain rates representative of traumatic impacts, as well as repetitive, sub-failure loading scenarios. By encompassing this wider range of loading rates, the research captures the dura mater's viscoelastic and strain-rate-dependent behaviors with greater fidelity.
- **Cyclic Loading Emphasis:** In contrast to most existing work that relies on single-cycle tests, this project will explore the Mullins effect and hysteresis through repeated tensile loading. By quantifying stress-softening and energy dissipation, the study provides deeper insight into how mechanical integrity evolves under repetitive or vibrational loading, conditions that may hold clinical, occupational, or sports relevance. This focus on cyclic behavior moves beyond simple failure metrics to reveal dynamic changes in tissue properties.
- **Advanced Imaging and Strain Measurement:** The integration of DIC techniques will allow high-resolution strain mapping of thin, heterogeneous tissues such as the spinal dura. Although DIC has been applied in a limited number of studies, it is rarely combined with multi-rate and cyclic loading, making this investigation especially rigorous. The resulting data on local strain distributions and apparent Poisson's ratio will be key to constructing accurate computational models.
- **Refined Constitutive Modeling and HBM Integration:** Using robust experimental data, the project will formulate and implement a visco-hyperelastic or transversely isotropic constitutive law that captures the dura's nonlinear, rate-sensitive response. Unlike the linear-elastic formulation in HBM (THUMS), this approach accounts for viscoelastic effects, including stress-softening and hysteresis. Integrating these refined tissue models into HBMs promises to enhance the predictive power of FE simulations in crashworthiness studies, neurosurgical planning, and medical device evaluation.

Collectively, these novel elements are poised to bridge significant knowledge gaps concerning spinal dura mater behavior in multiple loading scenarios. The outcomes will not only advance fundamental biomechanics but also support clinical strategies and engineering designs aimed at protecting spinal cord integrity.

### 2.4 Impact of the project results on the development of the research field and scientific discipline

The expected outcomes of this project offer significant potential for advancing current understanding and modeling capabilities of spinal dura mater mechanics. These findings will influence biomechanics, clinical practice, and road safety, generating impacts across multiple scientific and technical areas:

- **Mechanical Data:** The focus on uniaxial tensile (low and high-rate) and cyclic (Mullins effect, and hysteresis) tests with DIC (optical extensometers in two directions) will produce a dataset describing the dura's viscoelastic behavior under realistic conditions, supporting the development of advanced constitutive models for soft tissues. Such findings will also inform future research on injury and protection of spinal cord or surgical interventions (e.g., implants).

- **Interdisciplinary Collaboration:** By combining experimental biomechanics, advanced imaging techniques, and FE modeling, the project will foster a multidisciplinary framework. This collaboration expands the skill sets and methodological range within biomechanics while encouraging partnerships with fields such as, materials science, and medical imaging.
- **HBMs Refinement:** By incorporating a more accurate, rate-sensitive, and cyclically validated dura mater model, this project will enhance widely used HBMs, which have thus far relied on simplified or purely elastic assumptions for soft tissues. This refinement leads to more reliable injury predictions in numerical crash testing.
- **Evidence-Based Knowledge Base:** The experimental and computational findings will give an information for future investigations, setting new standards in testing protocols, model validation, and multidisciplinary research. By offering these contributions, the project will serve as a reference in the field of spinal dura mater mechanics.

# 3 Work plan

## 3.1 General research plan

The project will be structured into several phases, each supported by a multidisciplinary of specialists in biomechanics, computational modeling, and clinical practice.

**Phase 1** involves securing ethical approvals, acquiring the requisite cadaveric specimens through an approved body donation program, refurbishing the existing dynamic testing machine, and preparing standardized spinal dura mater samples.

**Phase 2** encompasses the main experimental campaign, comprising a spectrum of cyclic tests (to observe hysteresis and the Mullins effect), uniaxial quasi-static and high-rate dynamic tests to capture the anisotropic and rate-dependent behavior of the tissue.

**Phase 3** addresses data postprocessing and analysis, applying signal filtering, parameter extraction, and statistical methods to organize the results.

**Phase 4** an anisotropic, visco-hyperelastic constitutive law is formulated and calibrated using the collected datasets, with particular attention to multi-directional behavior and time-dependent effects.

**Phase 5** integrates the validated model into LS-DYNA via user-defined subroutines and compares simulated outcomes with experimental measurements to ensure predictive accuracy.

**Phase 6** focuses on determining critical thresholds and injury risk metrics for dura mater compromise, ultimately informing guidelines for improved safety measures, clinical procedures, and broader protective strategies.

## 3.2 Specific research objectives and tasks

All phases within all PGs will be intricately connected, necessitating continuous information sharing (see **Fig. 1**).

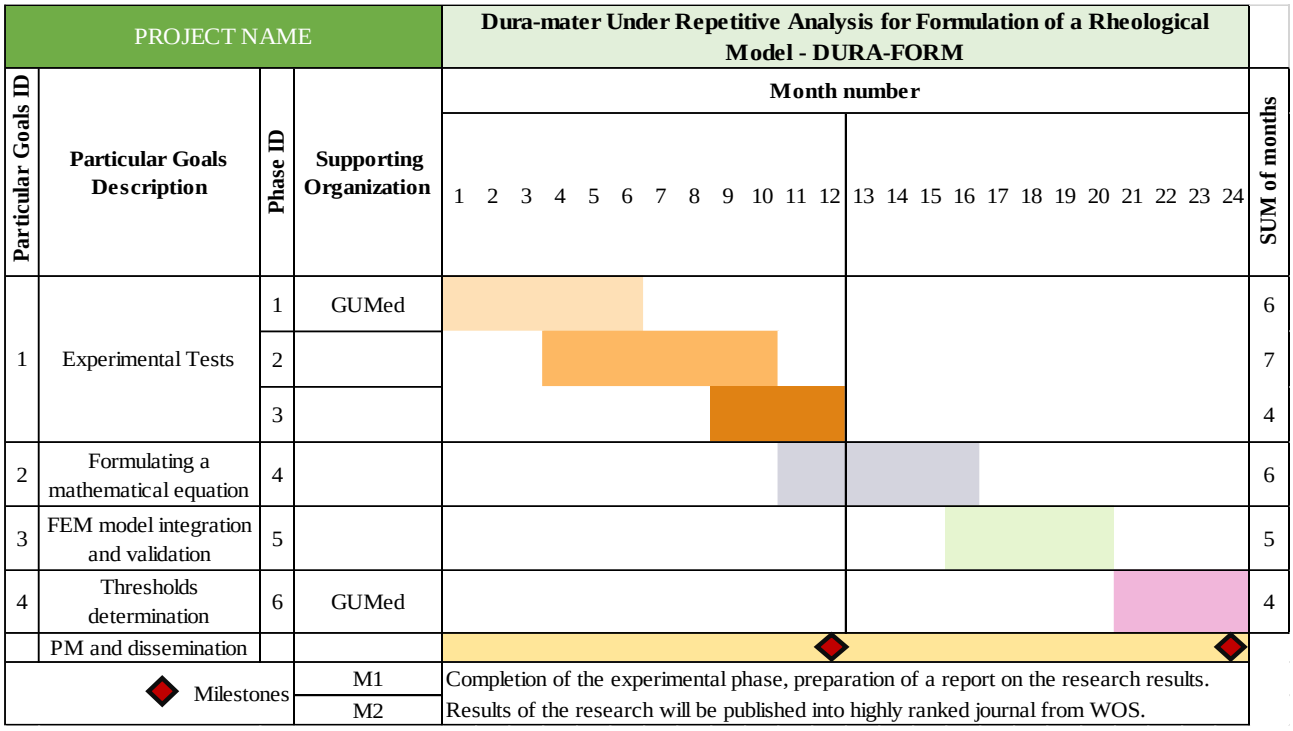


**Fig. 1** Gantt chart: Time schedule of work packages and tasks (Color intensity differentiates tasks)

## PG1: Experimental Characterization of the Spinal Dura Mater

**Phase 1** primary objective is to secure ethical approvals from institutional committees and acquire cadaveric donor material for spinal dura mater testing. The team will remove vertebral columns following standard dissection steps, preserving critical landmarks and minimizing tissue damage. This includes posterior incisions, careful muscle detachment, and spinal cord extraction to expose the dura. Once harvested, each dural sheet will be rinsed in saline, checked for pathologies, and labeled by anatomical region. Simultaneously, the dynamic testing machine will undergo refurbishment to handle diverse loading rates. Load cells will be recalibrated, software updated, and the environmental chamber's temperature-humidity controls validated. By establishing consistent specimen preparation and verifying equipment performance, Phase 1 lays a foundation for reliable experimentation. Adhering to strict protocols and ethical guidelines ensures data quality and reproducibility, setting the stage for **Phase 2**'s cyclic and uniaxial evaluations. Additionally, initial training sessions will be conducted to ensure all personnel follow standardized sample-handling protocols and safety measures.

**Phase 2** aims at the systematic mechanical testing of prepared dura mater samples. First, cyclic loading protocols are applied to investigate the Mullins effect, hysteresis loops, and stress-softening under repeated sub-failure strains. Each specimen will be mounted in a universal testing machine, placed in a controlled environment at physiological temperature and humidity, and subjected to incremental cyclic loads until a stable hysteresis is achieved. Next, quasi-static uniaxial tension tests are to be conducted to map full stress–stretch relationships and to estimate the apparent Poisson's ratio, especially across different anatomical orientations. Finally, high-rate tensile tests will capture the tissue's response to dynamic loading scenarios, utilizing the refurbished apparatus capable of strain rates up to 50 $s^{-1}$. Throughout this phase, force, displacement, and optical strain measurements (via DIC) will be recorded, ensuring comprehensive characterization. The resulting dataset will provide baseline information on rate sensitivity, anisotropy, and potential preconditioning effects.

**Phase 3** focuses on the postprocessing and interpretation of experimental data acquired in **Phase 2**. Recorded force–displacement signals will undergo filtering using standardized approaches, such as low-pass Butterworth techniques, to remove high-frequency noise and clarify stress–stretch profiles. Statistical methods, including the Shapiro–Wilk and Mann–Whitney tests, will be used evaluate normality and compare mechanical parameters (e.g., failure stress, failure stretch, and elastic modulus) across various loading rates and anatomical regions. Where applicable, multiple comparisons will be adjusted using Bonferroni corrections to maintain rigor in hypothesis testing. This phase also examines local strain distributions obtained from DIC, refining estimates of apparent Poisson's ratio and assessing tissue anisotropy. Observations of microstructural damage, gathered from microscopic inspections, are integrated into the statistical narrative. By consolidating these findings into a unified database, **Phase 3** prepares a dataset that will inform constitutive modeling and subsequent FE analyses in **PG2** and **PG3**.

**Success Metrics for PG1**:

- Successful completion of ethical approvals, specimen procurement, and standardized sample preparation.
- Generation of cyclic, low-rate, and high-rate test data reflecting anisotropic and rate-sensitive dura behavior.
- Verification that hysteresis loops and Mullins effect trends are reproducible across specimens.
- Comprehensive database of mechanical parameters, including stress–stretch curves and failure metrics, suitable for constitutive modeling.

**PG2: Constitutive Model Formulation**

**Phase 4** focuses on formulating and calibrating a visco-hyperelastic constitutive model for the spinal dura mater, grounded in the empirical data from **PG1**. The approach combines an isochoric and volumetric hyperelastic component with rate-dependent viscous terms to reflect the tissue's anisotropy and dynamic response. Anisotropy arises from the directional arrangement of collagenous and elastic fibers in the dura mater, which leads to different mechanical responses depending on the loading direction. Python-based scripts will be developed to fit the model parameters across multiple strain rates, capturing both low- and high-speed deformation behaviors. To ensure validity, the Mullins effect and hysteresis observations from cyclic experiments will inform how the model addresses stress-softening phenomena. Numerical regression techniques, such as least squares methods with trust-region reflective optimization, will yield best-fit parameters and quantify confidence intervals. Parametric studies will be conducted to assess sensitivity, evaluating the impact of fiber orientation, volumetric constraints, and frictional losses on stress–stretch curves. By concluding **Phase 4**, a mathematical framework will be ready to drive FE simulations in **PG3**.

**Success Metrics for PG2:**

- Effective incorporation of anisotropy, and rate dependence within the constitutive law.
- Achieved high correlation (e.g., $R^2 > 0.95$) when fitting model parameters to stress–stretch data at multiple strain rates.
- Demonstrated consistency in predicted transverse behavior (apparent Poisson's ratio) compared with DIC measurements.
- Confirmation that the final model is stable and suitable for FE analysis in **Phase 5**.

**PG3: Numerical Integration and Validation**

**Phase 5** concentrates on implementation of the new material law into a commercial FE software (ANSYS LS-DYNA) via a user-defined subroutine. The process comprises coding the constitutive equations, including hyperelastic, anisotropic, volumetric, and viscous components, in Fortran language. Single-element benchmark simulations will be then executed to validate the implementation against analytical solutions, verifying correct stress updates under uniaxial tension. Once validated, the FE model will replicate the **Phase 2** experimental setup, applying boundary and loading conditions identical to laboratory tests. Force–displacement curves, and strain distributions (DIC) from simulated analyses will be compared to measured data, evaluating predictive accuracy across various strain rates.

**Success Metrics for PG3:**

- Benchmark tests that closely match analytical solutions (±10% error) in single-element cases.
- High correlation ($R^2 > 0.95$) between FE predictions and experimental force–displacement data across multiple strain rates.

**PG4: Injury Risk Metrics and Recommendations**

**Phase 6** integrates the validated FE model with experimentally derived mechanical parameters, such as failure stress, failure strain, and elastic modulus, to establish practical injury risk metrics for the spinal dura mater. Using these measured thresholds, the project refines predictive models in human body simulations, ensuring that high-impact or repetitive loading scenarios accurately account for observed tissue tolerance levels. Comparative analyses will map how specific mechanical parameters influence predicted damage patterns under varying strain rates, guiding the identification of compromise thresholds. By correlating simulation outcomes with experimental rupture data, this phase generates risk curves or limit values that can be embedded in occupant safety models or medical materials. Clinical collaborators will review these findings to validate physiological plausibility. **Phase 6** concludes by merging computational and experimental results to propose failure thresholds for the spinal dura, both for numerical analyses in HBMs and for the development of medical materials.

**Success Metrics for PG4:**

- Quantitative injury thresholds based on experimentally confirmed failure stress, failure strain, and elastic modulus.
- Proposition of validated material law and parameters for integration into occupant restraint models (e.g., HBMs).

### 3.3 State of preliminary and initial research

Within the framework of the Argentum project (GdanskTech 27/1/2022/IDUB/13b/Ag), entitled *Development of anisotropic, visco-hyperelastic constitutive law for modeling spinal dura mater of humans*, over 200 uniaxial tensile tests of human spinal dura mater were conducted in both quasi-static (approximately 0.0042 $s^{-1}$) and dynamic (up to 25 $s^{-1}$) regimes. The study accounted for multi-directional anisotropy encompassing various fiber orientations and donor related demographic variability, capturing potential discrepancies in the tissue's mechanical response. Notable differences were observed in the elastic modulus and tensile strength, depending on fiber alignment (~283 MPa vs. ~16 MPa) and strain rate. Furthermore, the high apparent Poisson's ratio (occasionally exceeding 4) suggests volumetric changes, challenging the commonly held assumption of near-incompressibility of the dura mater.

The research employed DIC, compared with crosshead displacement measurements, resulting in a preliminary testing protocol tailored for thin biological tissues. Initial findings also indicate strong viscoelastic effects, especially at higher strain rates, highlighting the need for advanced constitutive models (e.g., visco-hyperelastic) to accurately describe tissue behavior.

On this basis, two publications (currently under review) have been prepared: the first addresses measurement and methodological challenges, while the second examines rate-dependent mechanical properties and introduces a preliminary visco-hyperelastic model. The results from both studies serve as a foundation for more extensive numerical validation, covering a variety of loading scenarios commonly associated with spinal injuries.

The Authors of the application conducted other preliminary studies for the purposes of this project, which concerned, inter alia, carrying out ligaments experimental studies, conducting and validation of numerical simulations, and analysis of the HBMs response. As part of previous research initiatives, a number of biomechanical experimental tests and simulations were conducted. These efforts led to several publications, such as [18,42,46–49].

In [18], the experimental investigation focused on the geometric and mechanical properties of human thoracic spine ligaments was presented. This research examined spine ligaments, including the anterior longitudinal, posterior longitudinal, capsular, ligamenta flava, and the interspinous and supraspinous ligament complex. Each ligament was subjected to preparation steps: dissection, reinforcement, and potting in epoxy resin. Then samples were subjected to uniaxial quasi-static tensile tests in a controlled environment (**Fig. 2B**). For this purpose, a custom-designed testing machine (Patent registration no. P.443948) was constructed (**Fig. 2A**). Additionally, the Authors investigated six cervical spine sections in a ROM tests (**Fig. 2C**). The experimental methodologies developed in this publication and conducted ROM tests form the foundation for the investigative approach of the current project.

Additionally, dynamic tensile tests were conducted at strain rates of 50/s for cervical ligaments (3 - 10mm length). Test is related to grant OPUS19 (2020/37/B/ST8/03231, National Science Centre of Poland). The current custom-designed (**Fig. 2A**) machine has limitations for higher strain rates (max velocity - 50cm/s). The current project plans to conduct dynamic tests on dura mater (~20mm sample length) at high strain rates (to 50/s), that may occur during sports activities, bungee jumping or during a car accident. This additional research will facilitate the development of a mathematical model, enhancing the accuracy of numerical models.

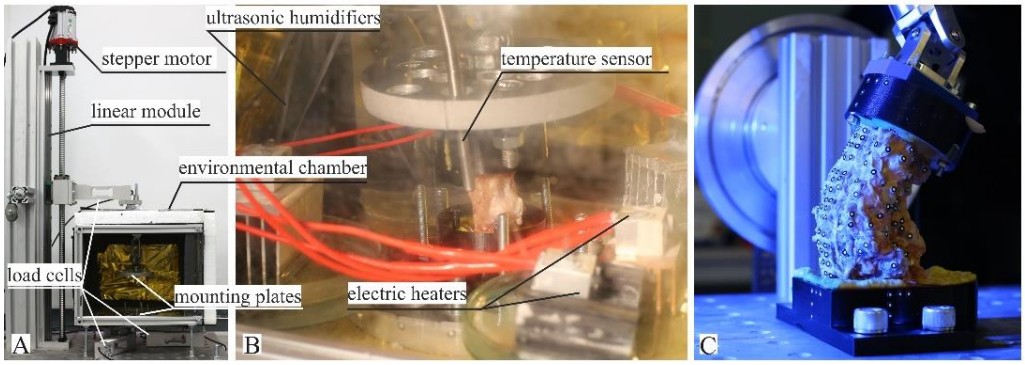


**Fig. 2** Experimental setup for tests: A. Custom-designed machine, B. Environmental chamber, and C. ROM with DIC measurement.

In [47], the authors simulated damage in fibrous connective tissues, such as tendons and ligaments, using the FEM within the Abaqus software. These tissues display hyperelastic behavior influenced by anisotropy from collagen fibers, making them challenging to study due to issues like damage and irreversibility during traumatic injuries. The developed model utilizes the UANISOHYPER_INV subroutine in Abaqus to simulate the hyperelastic and damage response of tissues. It modifies the constitutive law to include a damage function, reflecting the behavior of these tissues under loading close to rupture. The paper provides comprehensive details about the numerical implementation and incremental damage function calculation, aiming to facilitate the use of this modeling approach in biomechanical simulations.

Additionally, two papers considering the numerical material modelling of ligament tissues are being considered for publication. One paper presents the usage of UMAT procedure in ANSYS LS-Dyna program and comparison with the Abaqus Software. The second one presents the implementation of visco-hyperelastic model for soft tissue into UMAT procedure in LS-Dyna program and validation process of the obtained results.

Currently, the development of cervical spine FE model is being worked on **Fig. 3A**. The geometry was created in MIMICS software, based on CT and MRI scans. The models consist of 457668 nodes and 2379437 elements. The ligament material properties were derived from our previous experimental analysis. Other material properties are based on the literature analysis.

Another study that contributed to the current project is [46]. The authors carried out a case study on a specific L-Spine injury (**Fig. 3B**), which was the result of a road accident where a 2014 Honda Accord hit a concrete RSB under TB32 impact conditions. In addition, the HBM was also used, the displacements of which were extracted and then applied to an isolated model of the L-Spine from THUMS. The study analyzed various measures of damage of the vertebrae, e.g., using strain-based metrics [50] and a more general metric - lumbar spine index (LSI) [41]. These analyses indicated that it is a need to make some adjustments to the THUMS L-Spine model, that resulted in another publication in biomechanical area [42].

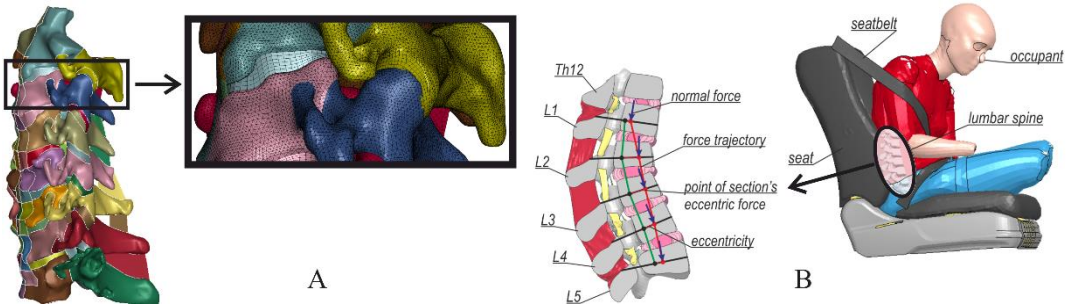


**Fig. 3** A. Figure of our cervical model, B. VIVA model form [51].

The analysis and development of THUMS L-Spine model (**Fig. 3A**) are presented in the work [42]. The focus was on enhancing the model's ability to accurately replicate the biomechanical behavior of the human L-Spine under various loading conditions. This involves integrating orthotropic and nonlinear material properties for ligaments and hyperelastic properties for the annulus fibrosus and nucleus pulposus. The modified model was subjected to different loading scenarios to measure intervertebral rotations and disc pressures. Results from these simulations showed good alignment with experimental data, demonstrating the model's potential for biomechanical research.

### 3.4 Risk analysis

The research team has experience in conducting biomechanical projects, during which many similar risks have been effectively identified and minimized. Established procedures and close team collaboration will allow achieving research objectives despite the listed potential risks.

| Risk | Probability | Impact | Mitigation Strategy |
|---|---|---|---|
| **(I) Technical Risks** | | | |
| Equipment failure/ damage | Mid | High | Regular equipment maintenance, staff training, using equipment according to its intended purpose. |
| Low quality of experimental data | Mid | High | Conducting pilot tests, staff training, ongoing quality control of results. |
| Loss of experimental data | Low | High | Regular backups (at least once a week) of data to research team servers and cloud storage (e.g., OneDrive). |

| | | | |
|---|---|---|---|
| Issues with data integrity and sharing | Low | Mid | Clearly defined data exchange protocols, regular team meetings, shared data platform (e.g., OneDrive), appointing a data manager. |
| Variability of sample properties | High | High | Application of statistical methods, increasing the number of samples, precise documentation. |
| Human sample damage | Low | High | Proper preparation and protection of samples, storage conditions adhering to current medical knowledge (e.g., maintaining humidity and temperature). |
| **(II) Financial Risks** | | | |
| Budget overrun | Low | High | Detailed budget plan based on current price offers, regular expenditure monitoring, reserve funds from indirect costs. |
| **(III) Workforce Risks** | | | |
| Delays in obtaining ethical approvals | Mid | High | Early submission of applications; dedicated person with experience in obtaining ethical permits. |
| Delays in sample preparation | Low | High | Staff training, early preparation of samples, adequate number of personnel for sample preparation, readiness of workspace and tools. |
| Delays in conducting experimental studies | Low | Mid | Well-planned schedule, taking into account sufficient time buffers for research, early preparation of equipment for research. |
| Delays or difficulties in developing numerical models | Low | Mid | Detailed work plan and task division, progress monitoring, employment of experts, computation on efficient computing clusters. |
| Delays in data sharing | Low | Mid | Defined data sharing protocols and clear deadlines for data transfer; schedule monitoring. |

## 4 Research methodology

It should be emphasized that research conducted at the Gdańsk University of Technology (GUT) requires close cooperation with the GUMed. Both the work conducted at the GUMed related to the collection of material requires the use of appropriate procedures and the consent of the bioethics committee, as well as the activities conducted as part of the project at GUT require such consent. The PI has experience in cooperation with the anatomy department at the GUMed. As part of this cooperation, the elements related to the collection of biological material, preparation of samples, will be carried out exclusively by trained employees of the anatomy department. Then the samples will be secured and prepared for transport. Then the biological material will be transported to the GUT, where strength tests will be carried out in an appropriately secured room, by trained personnel equipped with appropriate personal protective equipment (including masks, aprons, gloves). The tests will be carried out on dedicated strength machines intended exclusively for testing biological material, secured with foil for the duration of the tests, and under a microscope. After conducting the tests, the material will be catalogued and secured, and then transported back to the GUMed premises where it will be disposed of in accordance with the donation program.

### 4.1 Sample preparation

Spinal dura mater will be collected from five donors (approximately 50 to 80 years of age) through a body donation program approved by the Institutional Ethics Committee (Ordinance No. 26/2016, Medical University of Gdańsk, Poland). Based on GUMed's experience to date, this is realistic assumption within the timeframe set. Furthermore, limiting donor ages to this range exclude some undesirable age related changes. All donors will have provided informed consent for the scientific use of their bodies in accordance with ethically supervised protocols. An initial examination will be conducted to rule out soft tissue pathology, and basic information (age, sex, weight etc.) will be documented for each donor.

The vertebral columns will be removed via a posterior approach. Two longitudinal skin incisions, each placed roughly 30–40 mm lateral to the posterior midline, will extend from the occipital bone to the sacrum. The resulting skin flap, along with subcutaneous tissue, will be dissected and removed. Dorsal muscles will be detached from their cranial attachments at the skull, and dorsal extensor musculature will be systematically stripped from the spinous processes. Subsequently, the atlanto-occipital and sacroiliac joints will be severed.

The ribs will be cut approximately 10 mm lateral to the transverse processes, and the sacrum will be transversely sectioned at the S2/S3 level. The quadratus lumborum muscles will also be excised. Following these procedures, the entire vertebral column will be extracted and inspected from the ventral (abdominal) aspect.

After extraction, each vertebral column will be rinsed three times with chilled (~6°C) 0.9% saline, with each rinse lasting 15 minutes. Residual short muscles and rib fragments at the costovertebral joints will be removed. The vertebral column will then be segmented into cervical, thoracic, and lumbar regions. The dural cuffs at each intervertebral foramen, together with the associated spinal nerve roots, will be trimmed. Using a MacDonald dissector, the dura mater will be separated from the vertebral canal walls. Once the spinal cord complex is removed, the remaining vertebrae will be reserved for other examinations. The dura mater will then be rinsed again in physiological saline (see **Fig. 4**A), opened longitudinally along the stumps of the left nerve roots, and the spinal cord (with its pia and arachnoid maters) will be extracted (see **Fig. 4**B). Finally, the exposed dural sheet will be trimmed into rectangular pieces (approximately 10 × 35 mm) from anterior, posteriori, lateral sides, and some circumferentially (see **Fig. 4**C). **Fig. 4** illustrates the final steps in preparing the tissue samples.

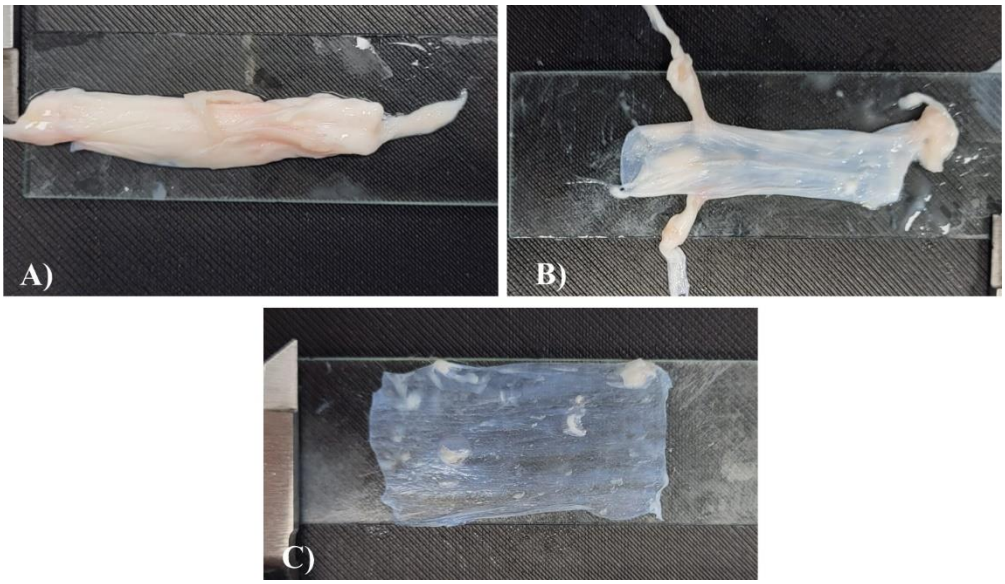


**Fig. 4** Dura mater sample preparation process: A) with accompanying tissues, B) without spinal cord, C) cleaned and cut. (*Example shown is from an animal model.*)

A custom 3D-printed forming-and-mounting adapter will be used to achieve standardized dog-bone geometry (**Fig. 5** and **Fig. 6**). The adapter will comprise two interlocking halves: a lower part featuring convex, pyramid-textured surfaces (**Fig. 5B** and **Fig. 6A**) and an upper part with matching concave pyramids (**Fig. 5A** and **Fig. 6B**). This complementary surface relief will improve grip integrity and positional repeatability during tensile loading. Two adapter types will be utilized: **Type 1** (**Fig. 5**) is designed for installation in a dynamic testing machine, while **Type 2** (**Fig. 6**) is configured for use in a commercial quasi-static and rheological testing machine.

Each rectangular dura sample will be placed on the concave half of the adapter and secured with cyanoacrylate within the designated mounting zone. The convex half, also coated with the adhesive, will then be aligned and pressed onto the tissue to create a uniform adhesive layer. Once the adhesive has fully cured, a scalpel will be used to trace the adapter's perimeter and excise the specimen to its final dog-bone outline. The central break-away portion of the adapter will subsequently be removed.

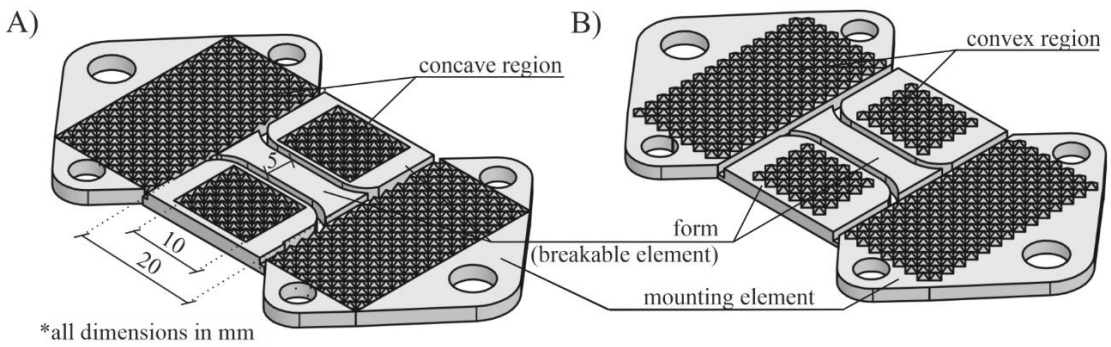


**Fig. 5** 3D-printed adapter Type 1: A) concave form, B) convex form.

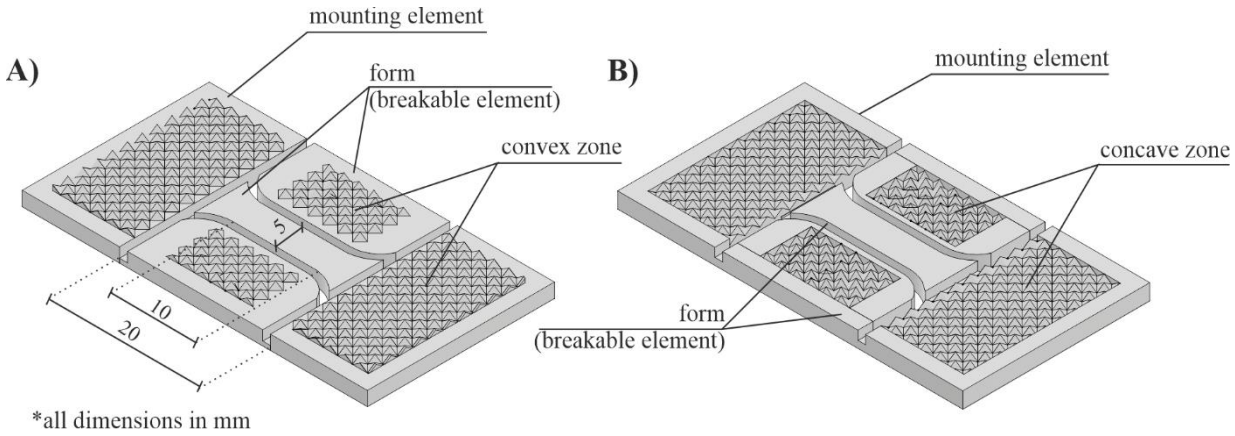


**Fig. 6** 3D-printed adapter Type 2: A) convex form, B) concave form.

Prior to testing, the thickness of each sample will be measured in triplicate using an electronic caliper (±0.01 mm precision). The readings will then be averaged. Initial width ($w_0$) and gauge length ($l_0$) (grip-to-grip distance) will be determined from calibrated photographs, analyzed in CAD software (AutoCAD, Autodesk, USA). In each photograph, longitudinal reference lines will define the length and transverse lines will define the width (**Fig. 7**). The mean values from these measurements will be documented as the specimen's starting dimensions. In addition, a photo of the optical microscope image of each sample will be taken.

Based on experience, it is estimated that about 250 specimens will be prepared in this way, including 200 specimens sectioned along the spine and 50 specimens sectioned circumferentially. In preliminary studies, the dura mater was divided into cervical, thoracic and lumbar sections, with the cervical and lumbar sections yielding an average of 15 specimens and the thoracic section alone yielding up to about 30, due to its greater length. It is assumed that five cadavers will allow the preparation of a total of about 300 specimens, but due to the risk of about 15% damage during preparation, this number was reduced to about 250. This sample size is deemed sufficient for comprehensive statistical analysis and crucial parameter estimation.

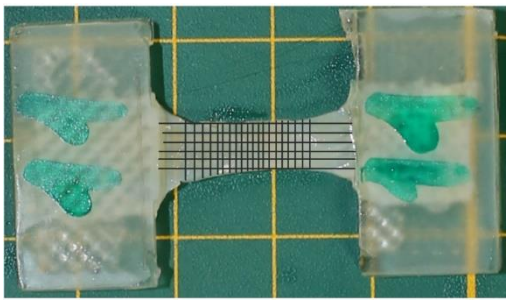

**Fig. 7** Determination of the initial length and width in a CAD environment.

***This stage will be carried out in close cooperation with GUMed.**

### 4.2 Constant cyclic test - hysteresis range identification

Three groups of 15 dog-bone dura mater specimens will be subjected to cyclic tests at stretch levels of 5%, 10%, and 15% of $l_0$ with each test performed at a frequency of 1 Hz. During testing, the specimens will be placed in an environmental chamber maintained at 36.6 °C and 99% relative humidity. Experiments will be conducted on a Zwick/Roell Z10 universal testing machine (**QSTM**, available in the department) equipped with screw grips (**SG**) (type 8133; Zwick/Roell GmbH & Co. KG, Ulm, Germany). The stress–stretch curves will be monitored in real time, and cyclic loading for each group will continue until the hysteresis loop stabilizes in the subsequent ten cycles (peak stress difference between cycles <1%), indicating that further changes in the stress–stretch relationship no longer occur.

Upon completion of this phase, the resulting data will be used to determine both the appropriate duration of preconditioning and the stretch range required for subsequent mechanical tests. Finally, all specimens will be examined under an optical microscope with comparison with reference photos to identify any visible microstructural alterations associated with the stabilized hysteresis response.

### 4.3 Cyclic test with increasing load amplitude - recognition of the Mullins effect

45 samples will be painted with a speckle pattern, and then two representative black ink markers will be placed on the surface of each sample to facilitate organoleptic tracking of local deformations, and using the DIC system (ARAMIS available in the department). Immediately prior to testing, samples will be mounted on a **QSTM** with **SG**, maintained in an environmental chamber at 36.6 °C and 99% relative humidity to minimize

tissue dehydration. Each specimen will be subjected to an incremental cyclic loading profile, beginning with a low force amplitude (0.5–5 N) and progressively increasing to higher amplitudes, while crosshead displacement and load are recorded continuously. After each increment, the load will be reduced to near zero to capture a complete loading–unloading cycle at every amplitude level. This procedure will be repeated until a maximum force amplitude of 0.5–25 N is reached or until the specimen ruptures. Based on preliminary studies and scientific literature, the tensile strength of dura mater can be approximately on average 25 MPa. The proposed amplitudes correspond to about 5-6 cycles to failure, which is sufficient to determine the Mullins effect [52].

Throughout the test, force, displacement, and strain (derived from the black ink markers or DIC data) will be recorded at a 50 Hz sampling rate. The resulting stress–stretch curves will then be analyzed to observe a softening that is characteristic to the materials exhibiting the Mullins effect, as evidenced by changes in the loading path for each successive cycle. In addition, specimens will undergo post-test observation via optical microscopy to document any local microstructural alterations that may have contributed to the observed stress–stretch behavior. This approach will enable the determination of how incremental loading impacts the mechanical response of the dura mater, providing insight into its capacity for deformation under repeated loading conditions.

### 4.4 Uniaxial quasi-static test

The test will be performed on samples formed longitudinally and transversely to the spine axis as well as transversely. 60 specimens will be tested on a **QSTM** mounted in **SG**. Immediately before loading, each specimen will be immersed in 0.9% saline at 36.6 °C, then clamped in the grips by its mounting elements (see Fig. 4A). A camera system (available in the department) will be used to record specimen stretching.

A preload of 0.5 N will be applied to specimens loaded in the longitudinal orientation, and 0.1 N will be applied to those loaded transversely. Following preloading, each specimen will undergo cyclic pre-conditioning to minimize hysteresis, with pre-conditioning parameters determined from the hysteresis-test results obtained in this project. Subsequently, a constant crosshead displacement rate of 5 mm $min^{-1}$ (≈ 0.0042 $s^{-1}$) will be imposed until specimen failure.

Force and crosshead displacement will be recorded at 50 Hz frequency, while digital-image correlation (DIC) images will be captured at 4 Hz frequency. Two optical extensometers (**Fig. 8B**), aligned with the longitudinal and transverse axes, will provide real-time measurements of longitudinal and transverse strains. All tests will be carried out in an environmental chamber maintained at 36.6 °C and 99% relative humidity.

The study will yield complete stress–stretch curves and time histories of both transverse and longitudinal strains. These data will be used to calculate various parameters, including the apparent Poisson's ratio.

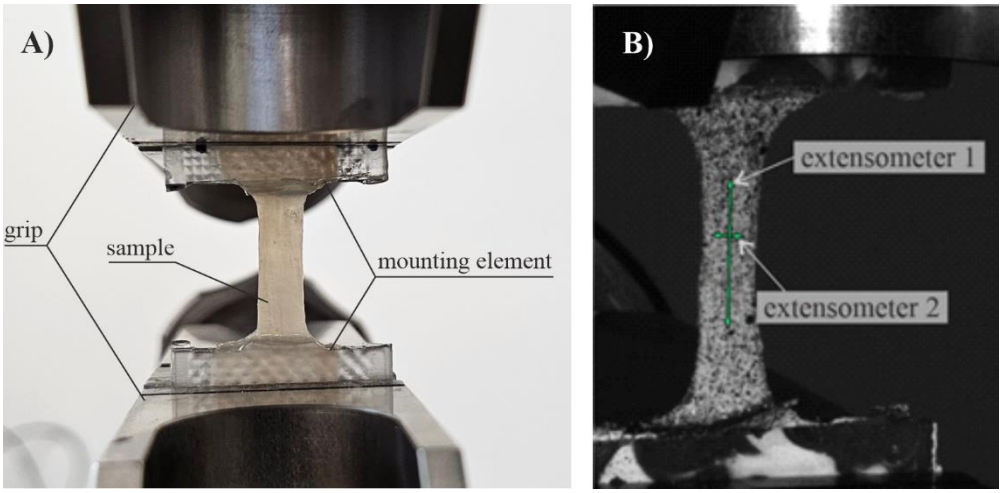


**Fig. 8** Sample: A) mounted in the testing machine, and B) with virtual extensometers marked

### 4.5 Uniaxial dynamic test

Uniaxial dynamic tensile tests will be carried out at four distinct strain rates ($0.5\ s^{-1}$, $10\ s^{-1}$, $25\ s^{-1}$ or $50\ s^{-1}$) using a custom-made dynamic testing machine (**DTM)** (Fig. 5A, patent application P.443948), modified to meet the requirements of this study. The system includes an AC stepper motor (Leadshine ELM-0400LH60F-SS-400W) operated by a servo controller (Leadshine ELP-RS400Z). Three bottom-mounted load cells (Utilcell M140; capacity up to 1500 N) will continuously record force. All tests will be conducted inside an environmental chamber maintained at 36.6 °C and approximately 95% relative humidity. There will be 100 samples for this purpose (25 for each strain rate).

Specimens will be elongated to complete rupture, with force and displacement data recorded at 5000 Hz using an HBM QuantumX MX840A system (Hottinger Baldwin Messtechnik, Germany) and Catman software. Modifications to the existing machine include replacing the stepper motor with a faster unit, adding a second column to increase structural stiffness, and rebuilding the absorber into a conical shape to damp rebound during impact. The environmental chamber will be adapted to accommodate the modified testing machine.

Prior to testing, each dura mater specimen will be mounted in the testing apparatus (**Fig. 8A** and **Fig. 9B**) using a custom 3D-printed adapter. A 0.5 N preload will be applied at a rate of $0.5\ s^{-1}$, followed by a 60-second relaxation period. Each specimen will then undergo a preconditioning phase consisting of 60 cycles at 5% strain and 1 Hz, after which it will rest for 60 seconds. Next, the rigid bracket (**Fig. 9A**) will be lowered to ensure sufficient distance for acceleration to the target velocity corresponding to the desired strain rate ($0.5\ s^{-1}$, $10\ s^{-1}$, $25\ s^{-1}$ or $50\ s^{-1}$). The proposed strain rates using statistical methods will allow determining the function of strain rate effect on the mechanical properties of the dura mater. The linear module control mechanism will accelerate the cantilever with bracket to this speed and maintain it until the specimen ruptures, then decelerate it to a complete stop.

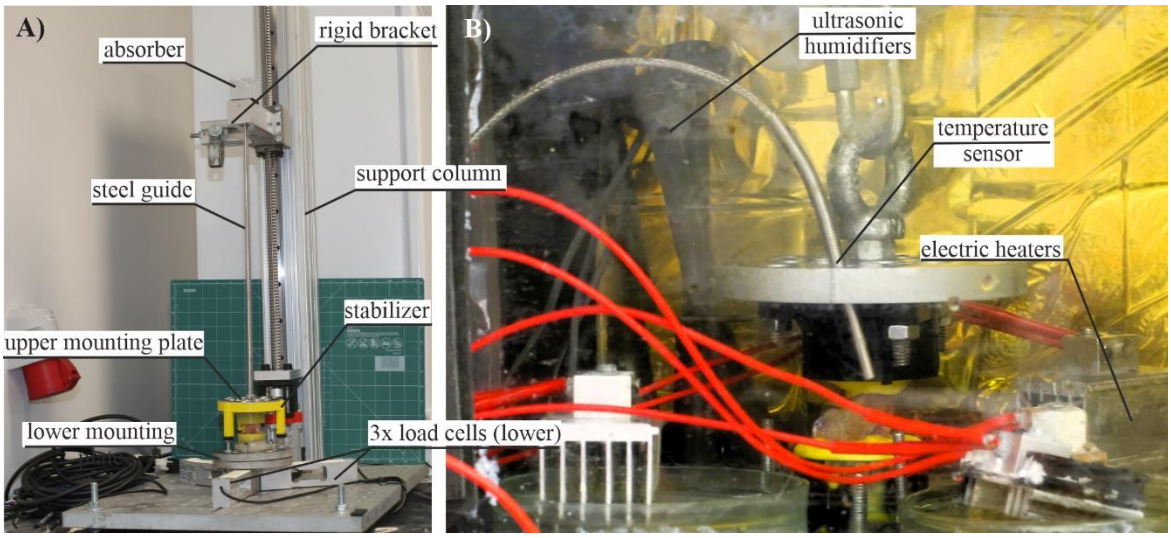


**Fig. 9** A) The custom-built testing machine and B) inside of environmental chamber

### 4.6 Analysis of uniaxial data

Experimental force-displacement data will be collected directly from each test. Initially, the raw signals will undergo filtering with a fifth-order, two-pole, low-pass Butterworth filter. Cutoff frequencies will be calculated as the values for which the cumulative sum of the energy spectral density of the force signal will reach 95% of the total energy, with a maximum value of 300 Hz imposed to take into account the physiological limitations of vibration transmission through soft tissues. The energy threshold determined following [53], while the upper limit of the cut-off frequency will be set to 300 Hz, as in SAEJ211 guidelines [54]. Then, the filtered force $F$ will divided by sample's initial cross-sectional area $A = wt$ to obtain the first Piola–Kirchhoff stress values, i.e., $P_{11} = \frac{F}{A}$. Stretch calculation from the initial ($l$) and deformed ($l + \Delta l$) specimen lengths according to $\lambda_1 = \frac{l+\Delta l}{l}$. These calculations will provide the full stress-stretch $P_{11}(\lambda_1)$ relationship, where the subscript denotes the direction of the applied displacement, which is aligned with the vertebral column axis. A typical tensile response for ligamentous tissue can be segmented into three distinct regions:

1. the toe region (from initial point to I transition point),
2. the linear region (from I to II transition point), and
3. the sub-failure region (from II transition point to the failure point).

To approximate the second region, the experimental curve will be searched to identify the longest segment that maintained a linear fit with $R^2 \cong 0.99$. The start of this segment will designated as I transition point, while the end as II transition point. The failure point is defined as the highest recorded stress value.

In order to obtain a representative average stress–stretch relationship for each strain rate, an averaging procedure will be carried out on the characteristic parameters derived from multiple experimental tests. The characteristic data points, i.e., stretch and stress values for the I transition, II transition, and failure points, will be averaged for each tested strain rate. A linear function will be then fitted between the averaged I and II transition points. Subsequently, a convex quadratic function will be introduced between the initial and the I transition points, maintaining $C^1$ continuity with the linear function and ensuring a non-decreasing trend.

Finally, a concave quadratic function will be defined between the second transition point and the failure point, preserving $C^1$ continuity with the linear region.

### 4.7 Mathematical description and numerical modeling of spinal dura mater

The human spinal dura mater can be represented as a composite material comprising an isotropic extracellular matrix (ECM) interspersed with a primary family of collagen fibers. The strain energy can be divided into two separate components: an isochoric $\psi^{\mathrm{e}}_{\mathrm{iso}}$ and volumentric $\psi_{\mathrm{vol}}(J)$ hyperelastic part, and a viscosity-related contribution $\psi^{\mathrm{v}}_{\mathrm{iso}}$.

The isochoric hyperelastic response $\psi^{\mathrm{e}}_{\mathrm{iso}}$, is separated into a matrix term $\psi^{\mathrm{e}}_{\mathrm{m}}(\bar{I}_1, \bar{I}_2)$, fiber term $\psi^{\mathrm{e}}_{\mathrm{f}}(\bar{I}_4)$ and to capture finite volumetric changes and large Poisson's ratios in soft tissues, it will be included volumetric strain energy term $\psi_{\mathrm{vol}}(J)$. This approach follows the framework described by Swedberg et al. [55], who formulated a penalty-based constraint to enforce a desired Poisson's ratio response. By combining $\psi_{\mathrm{vol}}(J)$ with the isochoric matrix and fiber contributions, the model can predict significant transverse contraction (i.e., high apparent Poisson's ratios) and associated volumetric changes under tensile loading. The final hyperelastic free energy may be proposed as:

$$\psi^{\mathrm{e}}_{\mathrm{iso}}(\bar{I}_1, \bar{I}_2, J, \bar{I}_4) = \psi^{\mathrm{e}}_{\mathrm{m}}(\bar{I}_1, \bar{I}_2) + \psi_{vol}(J) + \psi^{\mathrm{e}}_{\mathrm{f}}(\bar{I}_4), \tag{1}$$

where $J = det(\mathbf{F})$ is the Jacobian of deformation gradient $\mathbf{F}$. The terms $\bar{I}_1 = \mathrm{tr}(\bar{\mathbf{C}})$, $\bar{I}_2 = \frac{1}{2}\left[\left(\mathrm{tr}(\bar{\mathbf{C}})\right)^2 - \mathrm{tr}\left(\overline{\mathbf{C}^2}\right)\right]$, $\bar{I}_4 = \mathbf{A}_0 : \bar{\mathbf{C}}$ represent isochoric invariants computed from right Cauchy-Green tensor $\bar{\mathbf{C}} = \bar{\mathbf{F}}^{\mathrm{T}}\bar{\mathbf{F}}$ for $\bar{\mathbf{F}} = J^{-\frac{1}{3}}\mathbf{F}$ and reference configuration fiber direction tensor $\mathbf{A}_0 = \mathbf{a}_0 \otimes \mathbf{a}_0$. This volumetric term may be calibrated by experimental measures of apparent Poisson's ratio, $\nu_{\mathrm{app}} = -\frac{\varepsilon_{\perp}}{\varepsilon_{\parallel}}$.

Strain-rate effects are incorporated via $\psi^{\mathrm{v}}_{\mathrm{iso}}$ [44,56,57], which reflects the dependence on $\dot{\bar{\mathbf{C}}}$:

$$\psi^{\mathrm{v}}_{\mathrm{iso}}(\bar{I}_1, \bar{J}_2, \bar{I}_4, \bar{J}_5) = \psi^{\mathrm{v}}_{\mathrm{m}}(\bar{I}_1, \bar{J}_2) + \psi^{\mathrm{v}}_{\mathrm{f}}(\bar{I}_4, \bar{J}_5), \tag{2}$$

where $\bar{J}_2 = \frac{1}{2}\mathrm{tr}\left(\dot{\bar{\mathbf{C}}}^2\right)$ and $\bar{J}_5 = \mathbf{A}_0 : \dot{\bar{\mathbf{C}}}^2$ are associated with the rate of deformation $\dot{\bar{\mathbf{C}}} = \dot{\bar{\mathbf{F}}}^{\mathrm{T}}\bar{\mathbf{F}} + \bar{\mathbf{F}}^{\mathrm{T}}\dot{\bar{\mathbf{F}}}$. Here, $\bar{J}_2$ and $\bar{J}_5$ capture the magnitude of $\dot{\bar{\mathbf{C}}}$ in both the isotropic matrix and the anisotropic fibers, ensuring a positive-definite dissipation potential.

For hyperelastic materials, the First Piola–Kirchhoff stress tensor $\mathbf{P}$ can be obtained by differentiating the free energy function $\psi$ with respect to the deformation gradient $F$ [58]:

$$\mathbf{P} = \frac{\partial \psi}{\partial \mathbf{F}} \tag{3}$$

In many constitutive models, $\psi$ is defined in terms of scalar invariants (e.g., $I_1$, $I_2$, $I_4$) or rate invariants (e.g., $J_2, J_5$), rather than directly in terms of $\mathbf{F}$. Thus, building on the general relationship given by **Eq. (3)**, the first Piola–Kirchhoff hyperelastic stress $P^e_{11}$ in the loading direction is obtained via the chain rule, while the viscous stress $P^v_{11}$ is similarly derived to account for rate-dependent effects [58]:

$$\begin{gathered} P^e_{11} = \frac{\partial \psi^{\mathrm{e}}_{\mathrm{iso}}}{\partial I_1}\frac{\partial I_1}{\partial \lambda} + \frac{\partial \psi^{\mathrm{e}}_{\mathrm{iso}}}{\partial I_2}\frac{\partial I_2}{\partial \lambda} + \frac{\partial \psi_{vol}}{\partial J}\frac{\partial J}{\partial \lambda} + \frac{\partial \psi^{e}_{\mathrm{iso}}}{\partial I_4}\frac{\partial I_4}{\partial \lambda}, \\ P^v_{11} = \frac{\partial \psi^{\mathrm{v}}_{\mathrm{iso}}}{\partial J_2}\frac{\partial J_2}{\partial \dot{\lambda}} + \frac{\partial \psi^{\mathrm{v}}_{\mathrm{iso}}}{\partial J_5}\frac{\partial J_5}{\partial \dot{\lambda}}, \\ P^{total}_{11} = P^e_{11} + P^v_{11}. \end{gathered} \tag{4}$$

To estimate the material parameters, a nonlinear regression will be conducted using Python's *scipy.optimize* module (least square function with trust-region reflective approach) with the experimental stress-stretch data at distinct strain rates up to the II transition point. In the literature, two main approaches to identifying hyperelastic and viscous parameters have been reported [56,59]. The first approach focuses on fitting each individual stress–stretch curve, enabling a detailed representation of each tested sample's mechanical response. The second approach relies on averaged curves [19], which better capture the overall material behaviour across multiple samples, thus yielding more generalized parameter estimates. By employing both strategies, it is possible to account for variability among individual specimens while also providing a representative fit for the material as a whole. The overall fit quality will be evaluated using the adj. $R^2$, the normalized root mean square error (NRMSE), and the normalized mean absolute error (NMAE).

The Mullins effect will be adopted as the classical Ogden–Roxburgh pseudo-elastic formulation [60], in which a single scalar damage variable $\eta$ continually degrades the deviatoric stiffness whenever the material is re-loaded beyond its previous peak. In this framework the total strain energy is augmented as:

$$U(\bar{\lambda}_\iota, J, \eta) = \underbrace{\eta\, \widetilde{U_{\mathrm{dev}}}(\bar{\lambda}_\iota)}_{\text{softened primary response}} + \underbrace{\phi(\eta)}_{\text{damage dissipation}} + \underbrace{\widetilde{U_{\mathrm{vol}}}(J)}_{\text{volumetric penalty}} .$$

where $\widetilde{U_{\mathrm{dev}}}(\bar{\lambda}_\iota)$ and $\widetilde{U_{\mathrm{vol}}}(J)$ are the original hyperelastic deviatoric and volumetric potentials (**Eqs. (1)** and **(2)**) and $\phi(\eta)$ is a monotonically increasing "damage energy" function chosen so that

$$\frac{\partial U}{\partial \eta} = \widetilde{U_{\mathrm{dev}}}(\bar{\lambda}_\iota) + \phi'(\eta)$$

vanishes on the primary loading path ($\eta = 1$).

Finally, the first Piola–Kirchhoff stress including Mullins softening is computed in the usual way

$$P = \frac{\partial U}{\partial \boldsymbol{F}} = \eta\, \widetilde{P_{\mathrm{dev}}}(\bar{\lambda}_\iota) + \phi'(\eta)\, \frac{\partial \eta}{\partial F} + \widetilde{P_{\mathrm{vol}}}(J)$$

where $\widetilde{P_{\mathrm{dev}}}$ and $\widetilde{P_{\mathrm{vol}}}$ are the deviatoric and volumetric stress contributions from the underlying hyperelastic model.

### 4.8 Implementation into FEM software

Within this task, the proposed constitutive model for the human spinal dura mater will be numerically implemented and tested. First, the material law will be coded in Fortran (UMAT) and integrated into ANSYS LS-DYNA for FE analyses. As an initial check, the model will be evaluated on simple single-element with triple symmetry boundary conditions to verify that the numerical implementation matches analytical solutions. Following these benchmark comparisons, the experimental setup numerical model will be done and validated against uniaxial experimental data, including deformation measurements obtained via DIC.

### 4.9 Statistical analysis

All statistical analyses will be performed in Python using the *statsmodels* module [61]. Normality of data will be assessed via the Shapiro–Wilk test; if the data will not consistently meet normality requirements, nonparametric methods will be used. Geometrical data of the spinal dura mater will be compared between anterior and posterior regions using the Mann–Whitney U test. Additionally, the Mann–Whitney U test will be employed to compare mechanical properties, such as failure stretch, stress, and elastic modulus, defined as the slope of the linear region of the stress–stretch curve (i.e., the ratio of the increment in stress to the increment in stretch), within each strain rate group (e.g., 0.5 $s^{-1}$ anterior vs. 0.5 $s^{-1}$ posterior).

In a separate analysis, the effect of strain rate on the mechanical behavior of the spinal dura mater will be examined. If the data will not meet normality assumptions of Shapiro-Wilk test, the Kruskal–Wallis test will be used to assess differences among three strain rate groups (0.5, 10, 25 and 50 $s^{-1}$), followed by Dunn's test with Bonferroni correction for post hoc comparisons. In this analysis, strain rate will serve as the independent variable, while the dependent variables will include the tissue elastic modulus and the failure point values for both stretch and stress.

## 5 Research team

| | Role | Scope of Work | Required Professional Qualifications |
|---|---|---|---|
| 1 | **Principal Investigator** | Conducts experimental investigations, material modeling, data analysis, and article writing. | Must hold an M.Sc. degree and be a Ph.D. student interested in biomechanical problems. Experienced in static and dynamic testing of materials and structures, digital signal processing, and proficient in Python. Must have authored JCR publications in FEM modeling and biomechanics. |
| 2 | Mentor | Responsible for project supervision, reporting, recruitment and supervision of contractors and students. | Must hold a Ph.D. degree with extensive experience in FE modeling and project management, publications in high-impact journals. |
| 3 | Co-Investigator | Involved in material modeling, data analysis, and article writing. | Must hold an M.Sc. degree and be a Ph.D. student interested in FEM modeling of biomechanical problems. Proficient in Fortran, ANSYS LS-DYNA, Python scripting, and MATLAB. Must have authored JCR publications in FEM modeling and biomechanics. |

## 6 Literature


[1] Ünal M, Sezgin AB. Dura Mater: Anatomy and Clinical Implication. J Behav Brain Sci 2021;11:239–47. https://doi.org/10.4236/jbbs.2021.1110019.

[2] Gray H. Gray's Anatomy: The Anatomical Basis of Clinical Practice. 42nd ed. Philadelphia: Elsevier; 2020.

[3] Szotek S, Dawidowicz J, Geniusz M, Kozak M, Łukomski R, Czogalla A. The biomechanical characteristics of spinal dura mater in the context of its basic morphology. Acta Bioeng Biomech 2021;23. https://doi.org/10.37190/ABB-01972-2021-02.

[4] Nagel SJ, Reddy CG, Frizon LA, Chardon MK, Holland M, Machado AG, et al. Spinal dura mater: biophysical characteristics relevant to medical device development. J Med Eng Technol 2018;42:128–39. https://doi.org/10.1080/03091902.2018.1435745.

[5] Kimmell K, Shakir H, Dayoub H, Sincoff E. Spinal dural attachments to the vertebral column: An anatomic report and review of the literature. Surg Neurol Int 2011;2:97. https://doi.org/10.4103/2152-7806.82990.

[6] Maikos JT, Elias RAI, Shreiber DI. Mechanical Properties of Dura Mater from the Rat Brain and Spinal Cord. J Neurotrauma 2008;25:38–51. https://doi.org/10.1089/neu.2007.0348.

[7] Dong R-P, Zhang Q, Yang L-L, Cheng X-L, Zhao J-W. Clinical management of dural defects: A review. World J Clin Cases 2023;11:2903–15. https://doi.org/10.12998/wjcc.v11.i13.2903.

[8] Yudoyono F, Pebrianto A. Dural tear with multiple nerve root entrapment simultaneously after unstable spine injury. Neurologico Spinale Medico Chirurgico 2021;4:7–10. https://doi.org/10.36444/nsmc.v4i1.134.

[9] Zhang Z-D, Zhao L-Y, Liu Y-R, Zhang J-Y, Xie S-H, Lin Y-Q, et al. Absorbable Artificial Dura Versus Nonabsorbable Artificial Dura in Decompressive Craniectomy for Severe Traumatic Brain Injury: A Retrospective Cohort Study in Two Centers. Front Surg 2022;9. https://doi.org/10.3389/fsurg.2022.877038.

[10] Patin DJ, Eckstein EC, Harum K, Pallares VS. Anatomic and Biomechanical Properties of Human Lumbar Dura Mater. Anesth Analg 1993;76:535???540. https://doi.org/10.1213/00000539-199303000-00014.

[11] Zarzur E. Mechanical properties of the human lumbar dura mater. Arq Neuropsiquiatr 1996;54:455–60. https://doi.org/10.1590/S0004-282X1996000300015.

[12] Runza M, Pietrabissa R, Mantero S, Albani A, Quaglini V, Contro R. Lumbar Dura Mater Biomechanics. Anesth Analg 1999;88:1317–21. https://doi.org/10.1097/00000539-199906000-00022.

[13] Zwirner J, Scholze M, Waddell JN, Ondruschka B, Hammer N. Mechanical Properties of Human Dura Mater in Tension – An Analysis at an Age Range of 2 to 94 Years. Sci Rep 2019;9:16655. https://doi.org/10.1038/s41598-019-52836-9.

[14] Cavelier S, Quarrington RD, Jones CF. Tensile properties of human spinal dura mater and pericranium. J Mater Sci Mater Med 2022;34:4. https://doi.org/10.1007/s10856-022-06704-0.

[15] De Kegel D, Vastmans J, Fehervary H, Depreitere B, Vander Sloten J, Famaey N. Biomechanical characterization of human dura mater. J Mech Behav Biomed Mater 2018;79:122–34. https://doi.org/10.1016/j.jmbbm.2017.12.023.

[16] Mazgajczyk E, Ścigała K, Czyz M, Jarmundowicz W, Będziński R. Mechanical properties of cervical dura mater. Acta Bioeng Biomech 2012;14:51–8.

[17] Khadka N, Liu X, Zander H, Lee Bauer D, Pobiel B, Hilber K. Clinical Physics and Physiological Measurement To cite this article: R van Noort et al. vol. 2. 1981.

[18] Wolny R, Wiczenbach T, Andrzejewska AJ, Spodnik JH. Mechanical response of human thoracic spine ligaments under quasi-static loading: An experimental study. J Mech Behav Biomed Mater 2024:106404. https://doi.org/10.1016/j.jmbbm.2024.106404.

[19] Mattucci SFE, Cronin DS. A method to characterize average cervical spine ligament response based on raw data sets for implementation into injury biomechanics models. J Mech Behav Biomed Mater 2015;41:251–60. https://doi.org/10.1016/j.jmbbm.2014.09.023.

[20] Liber-Kneć, A., & Łagan S. The effects of preconditioning on tensile properties of pig's skin 2018;III:15.

[21] Diani J, Fayolle B, Gilormini P. A review on the Mullins effect. Eur Polym J 2009;45:601–12. https://doi.org/10.1016/j.eurpolymj.2008.11.017.

[22] Nitta N, Shiina T, Ueno E. Hysteresis parameter imaging of soft tissue under quasi-static deformation. IEEE Symposium on Ultrasonics, 2003, IEEE; n.d., p. 1606–9. https://doi.org/10.1109/ULTSYM.2003.1293216.

[23] Peña E, Peña JA, Doblaré M. On the Mullins effect and hysteresis of fibered biological materials: A comparison between continuous and discontinuous damage models. Int J Solids Struct 2009;46:1727–35. https://doi.org/10.1016/j.ijsolstr.2008.12.015.

[24] Tonge TK, Murienne BJ, Coudrillier B, Alexander S, Rothkopf W, Nguyen TD. Minimal Preconditioning Effects Observed for Inflation Tests of Planar Tissues. J Biomech Eng 2013;135. https://doi.org/10.1115/1.4025105.

[25] Tencer AF, Allen BL, Ferguson RL. A Biomechanical Study of Thoracolumbar Spine Fractures with Bone in the Canal. Spine (Phila Pa 1976) 1985;10:741–7. https://doi.org/10.1097/00007632-198510000-00009.

[26] Zwirner J, Ondruschka B, Scholze M, Thambyah A, Workman J, Hammer N, et al. Dynamic load response of human dura mater at different velocities. J Mech Behav Biomed Mater 2023;138:105617. https://doi.org/10.1016/j.jmbbm.2022.105617.

[27] Mattucci SFE, Moulton JA, Chandrashekar N, Cronin DS. Strain rate dependent properties of younger human cervical spine ligaments. J Mech Behav Biomed Mater 2012;10:216–26. https://doi.org/10.1016/j.jmbbm.2012.02.004.

[28] Bass CR, Lucas SR, Salzar RS, Oyen ML, Planchak C, Shender BS, et al. Failure properties of cervical spinal ligaments under fast strain rate deformations. Spine (Phila Pa 1976) 2007;32:7–13. https://doi.org/10.1097/01.brs.0000251058.53905.eb.

[29] Pearcy Q, Tomlinson J, Niestrawska JA, Möbius D, Zhang M, Zwirner J. Systematic review and meta-analysis of the biomechanical properties of the human dura mater applicable in computational human head models. Biomech Model Mechanobiol 2022;21:755–70. https://doi.org/10.1007/s10237-022-01566-5.

[30] Vergari C, Pourcelot P, Holden L, Ravary-Plumioën B, Gerard G, Laugier P, et al. True stress and Poisson's ratio of tendons during loading. J Biomech 2011;44:719–24. https://doi.org/10.1016/j.jbiomech.2010.10.038.

[31] Kohlhauser C, Hellmich C. Determination of Poisson's ratios in isotropic, transversely isotropic, and orthotropic materials by means of combined ultrasonic-mechanical testing of normal stiffnesses: Application to metals and wood. European Journal of Mechanics - A/Solids 2012;33:82–98. https://doi.org/10.1016/j.euromechsol.2011.11.009.

[32] Hammer N, Ondruschka B, Berghold A, Kuenzer T, Pregartner G, Scholze M, et al. Sample size considerations in soft tissue biomechanics. Acta Biomater 2023;169:168–78. https://doi.org/10.1016/j.actbio.2023.07.036.

[33] Jones DA, Gaewsky JP, Kelley ME, Weaver AA, Miller AN, Stitzel JD. Lumbar vertebrae fracture injury risk in finite element reconstruction of CIREN and NASS frontal motor vehicle crashes. Traffic Inj Prev 2016;17:109–15. https://doi.org/10.1080/15389588.2016.1195495.

[34] Zwirner J, Ondruschka B, Scholze M, Hammer N. Surface coating and speckling of the human iliotibial tract does not affect its load-deformation properties. Sci Rep 2020;10:20747. https://doi.org/10.1038/s41598-020-77299-1.

[35] Kim J, Gardiner SK, Ramazzotti A, Karuppanan U, Bruno L, Girkin CA, et al. Strain by virtual extensometers and video-imaging optical coherence tomography as a repeatable metric for IOP-Induced optic nerve head deformations. Exp Eye Res 2021;211:108724. https://doi.org/10.1016/j.exer.2021.108724.

[36] Bai P, Zhu F, He X. Optical extensometer and elimination of the effect of out-of-plane motions. Opt Lasers Eng 2015;65:28–37. https://doi.org/10.1016/j.optlaseng.2014.04.010.

[37] Genovese K, Badel P, Cavinato C, Pierrat B, Bersi MR, Avril S, et al. Multi-view Digital Image Correlation Systems for In Vitro Testing of Arteries from Mice to Humans. Exp Mech 2021;61:1455–72. https://doi.org/10.1007/s11340-021-00746-1.

[38] John J, Klug C, Kranjec M, Svenning E, Iraeus J. Hello, world! VIVA+: A human body model lineup to evaluate sex-differences in crash protection. Front Bioeng Biotechnol 2022;10:1–19. https://doi.org/10.3389/fbioe.2022.918904.

[39] Toyota Motor Corporation, Toyota Central R and D Labs. Inc. Documentation of Total Human Model for Safety (THUMS) AM50 Occupant Model Version 7.1. 2024.

[40] Li N, Fang H, Zhang C, Gutowski M, Palta E, Wang Q. A numerical study of occupant responses and injuries in vehicular crashes into roadside barriers based on finite element simulations. Advances in Engineering Software 2015;90:22–40. https://doi.org/10.1016/j.advengsoft.2015.06.004.

[41] Ye X, Gaewsky JP, Jones DA, Miller LE, Stitzel JD, Weaver AA. Computational modeling and analysis of thoracolumbar spine fractures in frontal crash reconstruction. Traffic Inj Prev 2018;19:S32–9. https://doi.org/10.1080/15389588.2018.1498090.

[42] Wiczenbach T, Pachocki L, Daszkiewicz K, Łuczkiewicz P, Witkowski W. Development and validation of lumbar spine finite element model. PeerJ 2023;11:15805. https://doi.org/http://doi.org/10.7717/peerj.15805.

[43] Upadhyay K, Subhash G, Spearot D. Visco-hyperelastic constitutive modeling of strain rate sensitive soft materials. J Mech Phys Solids 2020;135:103777. https://doi.org/10.1016/j.jmps.2019.103777.

[44] Limbert G, Middleton J. A transversely isotropic viscohyperelastic material: Application to the modeling of biological soft connective tissues. Int J Solids Struct 2004;41:4237–60. https://doi.org/10.1016/J.IJSOLSTR.2004.02.057.

[45] Zheng J, Tang L, Hu J. A Numerical Investigation of Risk Factors Affecting Lumbar Spine Injuries Using a Detailed Lumbar Model. Appl Bionics Biomech 2018;2018:1–8. https://doi.org/10.1155/2018/8626102.

[46] Pachocki L, Daszkiewicz K, Łuczkiewicz P, Witkowski W. Biomechanics of Lumbar Spine Injury in Road Barrier Collision–Finite Element Study. Front Bioeng Biotechnol 2021;9. https://doi.org/10.3389/fbioe.2021.760498.

[47] Sabik A, Witkowski W. On implementation of fibrous connective tissues' damage in Abaqus software. J Biomech 2023;157. https://doi.org/10.1016/j.jbiomech.2023.111736.

[48] Pachocki L, Fang H. Numerical modelling of different airbag folding patterns and their influence on occupant responses in frontal vehicle impact. International Journal of Crashworthiness 2024:1–16. https://doi.org/10.1080/13588265.2024.2348381.

[49] Bruski D, Pachocki L, Sciegaj A, Witkowski W. Speed estimation of a car at impact with a W-beam guardrail using numerical simulations and machine learning. Advances in Engineering Software 2023;184:103502. https://doi.org/10.1016/j.advengsoft.2023.103502.

[50] Hansson T, Keller TS, Panjabi MM. A study of the compressive properties of lumbar vertebral trabeculae: effects of tissue characteristics. Spine (Phila Pa 1976) 1986;11:1–7.

[51] Pachocki L, Daszkiewicz K, Łuczkiewicz P, Witkowski W. Biomechanics of Lumbar Spine Injury in Road Barrier Collision–Finite Element Study. Front Bioeng Biotechnol 2021;9:1–10. https://doi.org/10.3389/fbioe.2021.760498.

[52] Muñoz MJ, Bea JA, Rodríguez JF, Ochoa I, Grasa J, Pérez del Palomar A, et al. An experimental study of the mouse skin behaviour: Damage and inelastic aspects. J Biomech 2008;41:93–9. https://doi.org/10.1016/j.jbiomech.2007.07.013.

[53] Fazlali H, Sadeghi H, Sadeghi S, Ojaghi M, Allard P. Comparison of four methods for determining the cut-off frequency of accelerometer signals in able-bodied individuals and ACL ruptured subjects. Gait Posture 2020;80:217–22. https://doi.org/10.1016/j.gaitpost.2020.06.009.

[54] Society of Automotive Engineers. Instrumentation for Impact Test - Part 1 - Electronic Instrumentation. SAE J211-1 1995.

[55] Swedberg AM, Reese SP, Maas SA, Ellis BJ, Weiss JA. Continuum description of the Poisson′s ratio of ligament and tendon under finite deformation. J Biomech 2014;47:3201–9. https://doi.org/10.1016/j.jbiomech.2014.05.011.

[56] Jiang Y, Wang Y, Peng X. A Visco-Hyperelastic Constitutive Model for Human Spine Ligaments. Cell Biochem Biophys 2015;71:1147–56. https://doi.org/10.1007/s12013-014-0322-9.

[57] Zhurov AI, Limbert G, Aeschlimann DP, Middleton J. A constitutive model for the periodontal ligament as a compressible transversely isotropic visco-hyperelastic tissue A constitutive model for the

periodontal ligament as a compressible transverse. Comput Methods Biomech Biomed Engin 2007:37–41. https://doi.org/10.1080/13639080701314894.

[58] Holzapfel GA. Nonlinear Solid Mechanics: A Continuum Approach for Engineering. 1st ed. Chichester, West Sussex, UK: John Wiley & Sons; 2000.

[59] Trajkovski A, Omerović S, Hribernik M, Prebil I. Failure Properties and Damage of Cervical Spine Ligaments, Experiments and Modeling. J Biomech Eng 2014;136. https://doi.org/10.1115/1.4026424.

[60] Huang L, Yang X, Gao J. Pseudo-Elastic Analysis with Permanent Set in Carbon-Filled Rubber. Advances in Polymer Technology 2019;2019:1–8. https://doi.org/10.1155/2019/2369329.

[61] Seabold, Skipper and Perktold J. statsmodels: Econometric and statistical modeling with python 2010. www.statsmodels.org (accessed May 21, 2025).